Low-Operating-Voltage Organic Transistors Made of Bifunctional Self-Assembled Monolayers

ARTICLE *in* ADVANCED FUNCTIONAL MATERIALS · MARCH 2007

Impact Factor: 11.81 · DOI: 10.1002/adfm.200600179

DOI: 10.1002/adfm.200600179

Low-Operating-Voltage Organic Transistors Made of Bifunctional Self-Assembled Monolayers**

By *Mohammad Mottaghi*, *Philippe Lang*, *Fernand Rodriguez*, *Anna Rumyantseva*, *Abderrahim Yassar*, *Gilles Horowitz*,* *Stéphane Lenfant*, *Denis Tondelier*, and *Dominique Vuillaume*

Self-assembled monolayers (SAMs) are molecular assemblies that spontaneously form on an appropriate substrate dipped into a solution of an active surfactant in an organic solvent. Organic field-effect transistors are described, built on an SAM made of bifunctional molecules comprising a short alkyl chain linked to an oligothiophene moiety that acts as the active semiconductor. The SAM is deposited on a thin oxide layer (alumina or silica) that serves as a gate insulator. Platinum–titanium source and drain electrodes (either top- or bottom-contact configuration) are patterned by using electron-beam (e-beam) lithography, with a channel length ranging between 20 and 1000 nm. In most cases, ill-defined current–voltage (*I–V*) curves are recorded, attributed to a poor electrical contact between platinum and the oligothiophene moiety. However, a few devices offer well-defined curves with a clear saturation, thus allowing an estimation of the mobility: 0.0035 $cm^2 V^{-1} s^{-1}$ for quaterthiophene and 8×10^{-4} $cm^2 V^{-1} s^{-1}$ for terthiophene. In the first case, the on–off ratio reaches 1800 at a gate voltage of –2 V. Interestingly, the device operates at room temperature and very low bias, which may open the way to applications where low consumption is required.

1. Introduction

A recent trend in organic thin-film transistor (OTFT) is the reduction of the size of the device, for both its lateral dimension (source–drain distance) and thickness of the semiconductor and insulator layers. OTFT with a channel length L as short as 30 nm[1,2] and even 10 nm[3] have been reported. Such a reduction opens the way for devices operating at low bias. However, size reduction is hampered by the problem of contact resistance that rapidly limits the performance of the device. Ways of reducing the semiconductor thickness include the use of Langmuir–Blodgett (LB) films[4–6] and self-assembled monolayers (SAMs),[7,8] that is, molecular assemblies that spontaneously form when dipping the substrate into a solution of an active surfactant.[9] SAMs are now largely employed as a primer for the subsequent vapor deposition of the organic semiconductor, either on the insulator[10,11] or on the source and drain electrodes.[12] Much less work has been devoted to the use of SAMs as an active part of the OTFT, either as a gate dielectric[1,13] or as the semiconductor layer itself.[7,8] In the latter case, the current–voltage (*I–V*) curves did not allow quantitative extraction of the parameters of the device. Again, this can be ascribed to problems with contacts, but other reasons can be put forward, such as the poor long-order organization of the organic monolayer. The latter point is well illustrated by the work by Tulevski et al.,[8] where devices with $L > 60$ nm did not show any increase of the drain current (I_D) upon application of a gate voltage (V_G).

Here, we report on monolayer organic transistors made of bifunctional molecules that comprise a conjugated unit (terthiophene or quaterthiophene) connected to a short alkyl chain. In most cases, the devices showed output characteristics that did not allow clear parameter extraction. However, neat curves were obtained in a few cases, with mobility that fairly compares to that of the corresponding bulk oligothiophene.

2. Results and Discussion

2.1. Fabrication and Characterization of SAMs

Two routes were followed to fabricate the devices. In the first one, the molecule used was 8-methylether-*α*,*α*′-quaterthiopheneoctanoic acid (4T-MEOA), which comprises a short fatty acid group linked to a conjugated quaterthiophene (4T) moiety. The carboxylic acid end group was chosen because of its ability to initiate self-assembly on aluminum oxide.[14] Figure 1 outlines the synthetic pathway followed to obtain the molecule.

[*] Prof. G. Horowitz, M. Mottaghi, Dr. P. Lang, F. Rodriguez, Dr. A. Rumyantseva,[+] Dr. A. Yassar
ITODYS, CNRS-UMR 7086, University Denis-Diderot
1 rue Guy de la Brosse, 75005 Paris (France)
E-mail: horowitz@paris7.jussieu.fr
Dr. S. Lenfant, Dr. D. Tondelier, Dr. D. Vuillaume
IEMN, CNRS-UMR 8520
Avenue Poincaré, 59652 Villeneuve d'Ascq (France)
[+] Present address: LPICM, École Polytechnique, 91128 Palaiseau, France.

[**] We thank Dr. Hervé Aubin and Mr. Hatem Diaf for the deposition of alumina, Dr. Nordin Felidj and Mrs. Stéphanie Truong for AFM measurements, and the assistance of Mrs. Claude Charvy and Mr. David Clainquart for the mass spectroscopy characterization. We are grateful to François Tran Van and Claude Chevrot for the synthesis of the 3T compound. This work was supported by the French "Ministère délégué à L'Enseignement supérieur et à la Recherche" through contract ACI Nanosciences-Nanotechnology No. 02-2-0155. The IEMN group acknowledges IRCICA for partial financial support

ADVANCED FUNCTIONAL MATERIALS

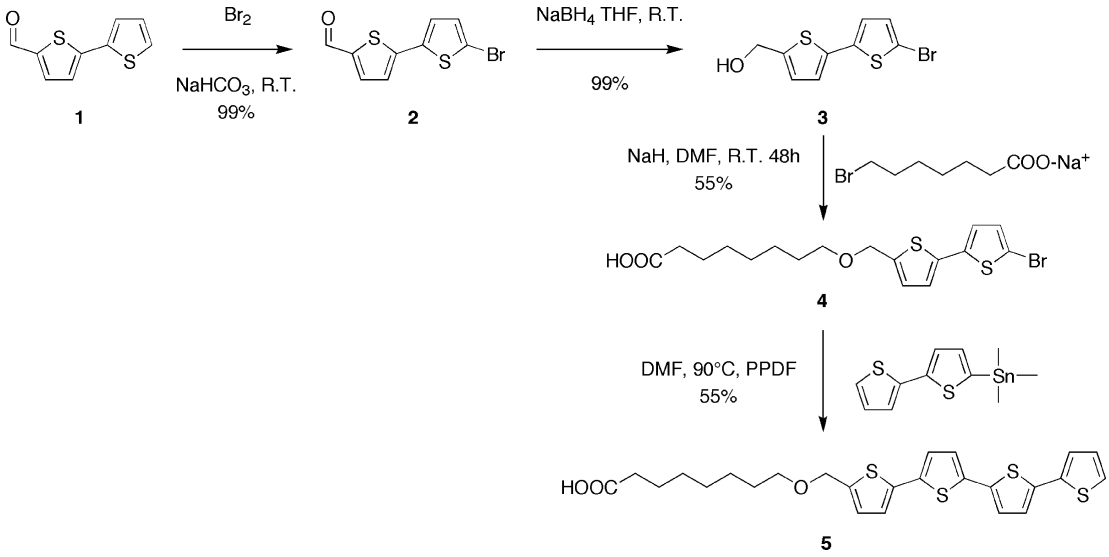

Figure 1. The figure outlines the synthetic pathway followed to synthesize the 8-methylether-α,α'-quaterthiopheneoctanoic acid **5** (4T-MEOA). The starting material, 5′-formyl-2,2′-bithiophene, is commercially available (Aldrich) or can be obtained by the formylation of the 2,2′-bithiophene. The bromination of the 5-formyl-2,2′-bithiophene with sodium bicarbonate and bromine at room temperature (R.T.) afforded the 5-bromo-5′-formyl-2,2′-bithiophene in quantitative yield. Sodium borohydride reduction of this intermediate in tetrahydrofuran (THF) led to 5-bromo-bithiophene-2-yl methanol. Alkylation in dimethylformamide (DMF) under typical Williamson ether conditions with the sodium salt of 6-bromooctanoic acid afforded the 2-bromo-2,2′-bithiophene-5-methylether octanoic acid **4**. The rigid conjugated core of quaterthiophene was built via a palladium-catalyzed Stille cross-coupling reaction between **4** and 5-trimethyltin-2,2′-bithiophene, with bis(triphenylphosphine)palladium(II) dichloride (PPDF) as a catalyst.

The ability of 4T-MEOA to self-assemble was first checked by dipping the cleaned alumina substrate in a benzene solution with a concentration varying from 10^{-4} to 4×10^{-4} M. Figure 2 shows atomic force microscopy (AFM) images and profiles of the SAM after various dipping times. Note that the average root-mean-square (RMS) roughness of the naked Al_2O_3 substrate compares with that of the underlying silicon wafer (around 0.2 nm).

After 45 s, the molecules form isolated grains of average height (1.6 nm) that cover 6 % of the total area. After 5 min, the coverage grows up to 80 %, and the average height to (2.7 ± 0.3) nm, close to the total length of the molecule, thus indicating that the molecules stand practically upright on the substrate. Complete coverage is achieved after 10 to 15 min. Beyond that time, the deposition of a second layer is observed, as evidenced by the measured thickness, suggesting that the deposition occurs layer by layer following a 2D process. We finally note that the film appears to be made of small grains of average diameter (25 ± 5) nm, which can be regarded as the size of the well-organized domains.

Further characterization was performed with polarization modulated IR reflection–absorption spectroscopy (PMIRRAS). The spectra in Figure 3 show the presence of the quaterthiophene moiety at 1503 cm^{-1} (C=C antisymmetric stretching ν_{as}, polarized along the long axis L of the molecule), 1445 and 1426 cm^{-1} (C=C symmetric stretching ν_s, polarized along the in-plane short axis M). The ratio $I(\nu_{as})/I(\nu_s)$ between the intensity of the bands is thirty times greater than that found in a KBr pellet, which indicates that the 4T moiety is oriented with an average tilt angle of 15° ± 5° with respect to the normal to the substrate.[15] Note the large feature locate around 1470 cm^{-1}, composed of carboxylate ν_s(COO–) and the C–C bands of the alkyl moiety, that partly obscures the quaterthiophene band.

For fabricating the transistors, we used an alternative "calibrated-drop-casting" technique, which consisted of adding with a calibrated syringe the exact amount of molecules needed to form one layer on top of the substrate. This technique presents the advantage of avoiding the formation of multilayers. We note that during the fabrication of the transistor structure, the channel area only experiences the deposition and lift-off of a lithographic resin, which cannot be thought of as liable to any significant modification of the surface. Moreover, just before the deposition of the SAM, the alumina was prepared following exactly the same procedure as for the samples used for characterization, so it appears reasonable to assume that the structure of the SAMs is identical in both cases. An additional thermal treatment (48 h at 50 °C under argon) helped in improving the quality (i.e., density and organization) of the SAM, as confirmed by contact angle and PMIRRAS measurements.

The alternative route consisted of fabricating the SAMs in a two-step process. In the first step, we formed a SAM of the alkyl chain, 10-undecenyl trichlorosilane ($SiCl_3$–$(CH_2)_9$–$CH=CH_2$). The vinyl end groups were further oxidized, thus promoting the attachment of the π-group (bis-(5,5″-(2-hydroxy 2-methylethyl))-2,2′:5′,2″-terthiophene (3T for short) by an esterification reaction. The reactions involved in the process are illustrated in Figure 4. Details on the synthesis, SAM formation, and characterization are given elsewhere.[16]

ADVANCED FUNCTIONAL MATERIALS

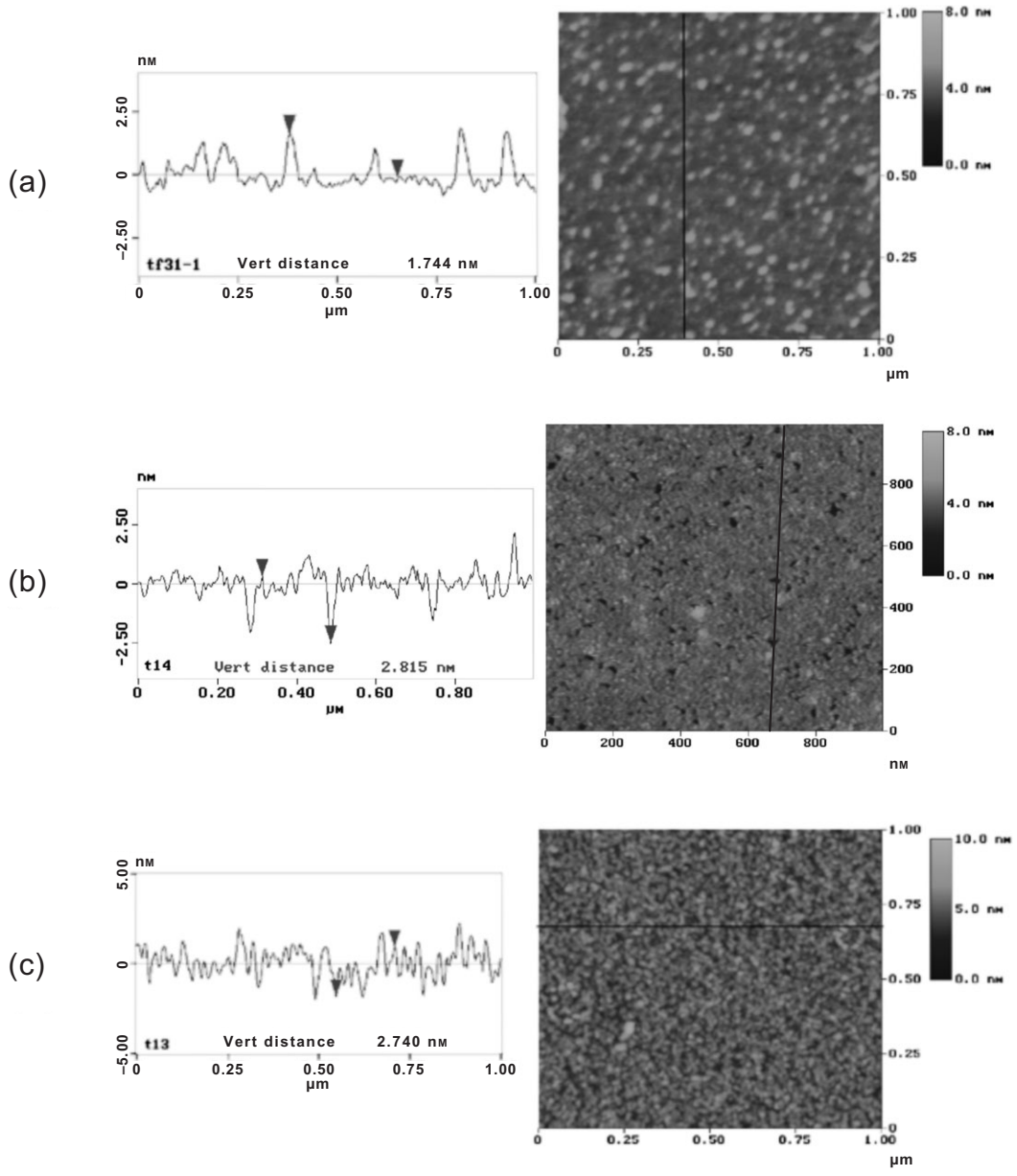

Figure 2. AFM image and profile of 4T-MEOA SAMs grown by dipping the Al_2O_3 substrate in a 4×10^{-4} M solution in benzene after various dipping times: a) 45 s; b) 5 min; and c) 20 min. The root-mean-square (RMS) roughness of the alumina substrate (not shown) was 0.2 nm.

2.2. Preparation of the Transistor Structures

The bottom-contact transistor structures were made before the deposition of the SAM by means of standard electron-beam (e-beam) lithography techniques following a process depicted in Figure 5. The structure was built according to an inverted (bottom-gate, bottom-source–drain contact) geometry on a highly doped p-type silicon wafer that acts as the gate electrode. Aluminum oxide was deposited in a homemade vacuum chamber by bombarding an aluminum target by an oxygen-ion beam, with a thickness in the range (100±25) nm, as measured by ellipsometry.

The platinum source and drain electrodes were formed by e-beam lithography in a poly(methyl methacrylate) (PMMA) resist. Metal (Ti/Pt; 2 nm:8 nm) was deposited using an e-beam evaporator in high vacuum followed by lift-off in acetone (Fig. 5b). The drawn channel length L varied between 50 nm and 1 μm, and its width W between 5 and 100 μm (with a constant W/L ratio of 100).

The next step was to produce large patterns (2400 μm × 600 μm) of silicon dioxide by plasma-enhanced chemical vapor deposition (CVD) to electrically insulate the contacts to be used with the probe station (Fig. 5c); the large contacts (Ti/Pt; 20 nm:200 nm) were patterned by e-beam lithography and deposited using an e-beam evaporator in high vacuum (Fig. 5d).

Optical and scanning electron microscopy (SEM) images of the final structure are displayed in Figure 6. The global (optical

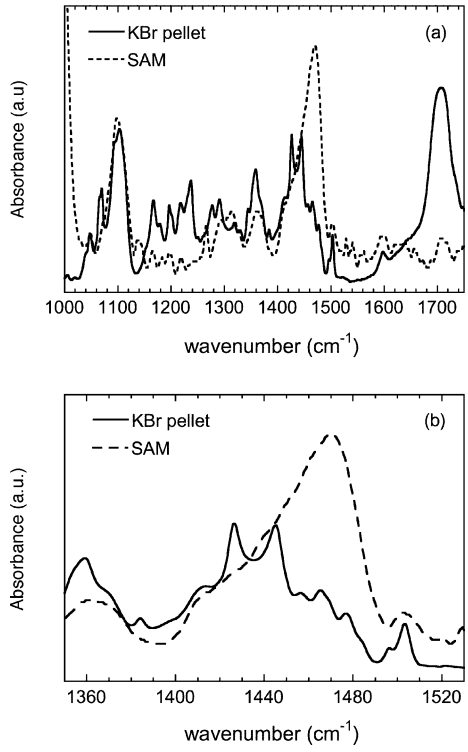

Figure 3. a) PMIRRAS spectrum of a 4T-MEOA SAM (dotted line) and IR spectrum of 4T-MEOA as a KBr pellet (solid line). b) Expansion of the spectrum in (a).

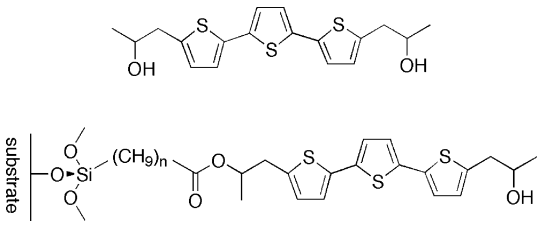

Figure 4. Chemical reactions involved in the fabrication of two-step SAMs.

microscope) view (Fig. 6a) shows the large contacts (200 μm × 200 μm) electrically isolated from the substrate (silicon covered with alumina) by the plasma silicon oxide. SEM images of the source–drain electrodes are shown in Figure 6b. The smallest interelectrode gap (15.7 nm) is magnified in Figure 6c. The reduced length compared to the drawn L (50 nm in this case) is attributed to the inhomogeneous thickness of the aluminum oxide. It is worth pointing out that, owing to the size of the well-ordered domains in the SAM (ca. 25 μm, see above), the number of domain boundaries along the path from source to drain does not exceed three.

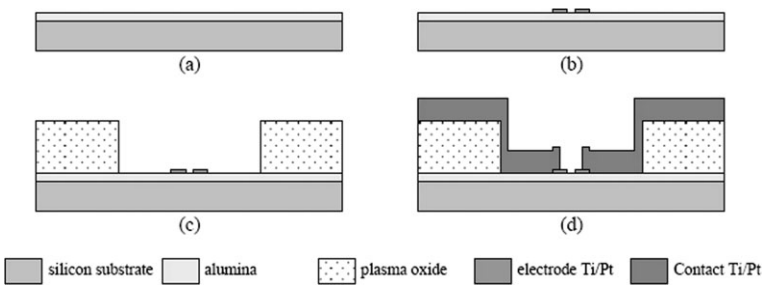

Figure 5. Main steps for source- and drain-contact fabrication. The structures were prepared on boron-doped Si wafers. a) Aluminum oxide deposition; b) e-beam lithography and lift-off of the source–drain electrodes; c) deposition of thick plasma CVD SiO_2; and d) e-beam lithography and lift-off of the large contacts for the probe station.

For the SAMs made with the two-step procedure, we used a top-contact structure with the same source and drain patterns as above. In this case, the gate dielectric was thermally grown silicon dioxide (10 nm thick), which allowed us to use SAMs based on trichlorosilanes. Trichlorosilanes are known to be more thermally stable (up to 350–450 °C)[17] than fatty acid SAMs on alumina. This was mandatory to insure that the SAM survives the annealing steps of the e-beam resist (170 °C during 30 min). The fabrication sequence is now (Fig. 5): growth of the 10 nm thick thermal silicon dioxide (Fig. 5a), formation of the large patterns of silicon dioxide (Fig. 5c), deposition of the large contacts (Fig. 5d), formation of the SAM (see above) and e-beam patterning of the source and drain electrodes (Fig. 5b). We confirmed that the SAM was still present after the latter process by measuring its thickness (ellipsometry) outside the channel area.

2.3. Characterization of the Transistors

As a preliminary remark, we note that all attempts with long channel devices ($L \geq 1$ μm) failed, thus confirming that a prerequisite for realizing a working monolayer OTFT is the reduction of the channel length to a size that compares to that of the well-organized domains of the SAM. This is in agreement with results reported by Tulevski et al.[8]

All the bottom-contact transistors were measured in ambient conditions. Out of the 25 fabricated devices, most of them did not give any signal. Four devices resulted in an output characteristic like that displayed in Figure 7. In all circumstances, the amplification was only obtained with negative gate bias, thus indicating that only injection of holes could be achieved. The nonlinearity of the current–voltage curves and absence of saturation are attributed to the poor quality of the contacts.

On two occasions, neat output and transfer characteristics as shown in Figure 8 have been recorded. We note that even in this case, the device had a tendency to degrade within a few hours once it was put into contact with air. This behavior has not been studied in more details. A tentative explanation is that in a monolayer device, the channel is in direct contact with air, which is at variance with conventional thin-film transistors where the channel is more or less protected by the thicker semiconductor film.

The following remarks can be made on the output characteristics in Figure 8a: The measurements were carried out over a restricted drain voltage V_D range (±0.5 V) because of leaks that appeared at higher V_D, presumably because of irregularities in the distance between source and drain, which could originate from the above-mentioned problem of electro-

ADVANCED FUNCTIONAL MATERIALS

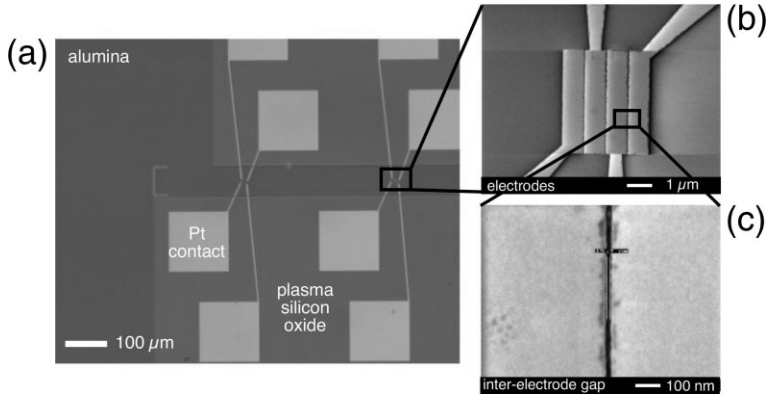

Figure 6. a) Optical microscopy image of the transistor. b) Scanning electron microscopy image of the source–drain region. c) Magnification of the shortest source–drain interelectrode spacing (ca. 16 nm).

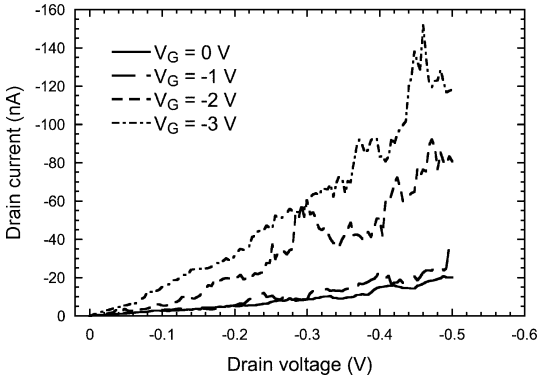

Figure 7. Output characteristic of a typical $Si/Al_2O_3/Pt/SAM$ transistor. The channel length is 20 nm, the channel width is 5 μm, and the gate dielectric capacitance 75 nF cm^{-2}.

migration. The mean current at zero bias is 8 pA, indicative of very low leakage through the insulator. In addition, the *I–V* curves are almost perfect straight lines close to the origin, providing evidence that the contact resistance is purely ohmic (i.e., it does not depend on the drain voltage); note that this does not necessarily imply that the contact resistance is negligible. Because of the limited range of the drain voltage, saturation is not reached in most of the curves. However, the enlarged view of the curve at $V_G = -0.5$ V displayed in the inset clearly shows saturation in this case. The curves in the inset also provide evidence that the device satisfactorily operates at drain and gate voltages as low as 0.5 V with an on–off ratio around 40. At $V_G = -2$ V (and $V_D = -0.5$ V) the on–off ratio attains 1800.

For a p-channel transistor with negligible contact resistance, the output characteristics can be described by the following equation

$$I_D = \frac{W}{L}\mu C_i \left[(V_G - V_T)V_D - \frac{V_D^2}{2}\right] \quad (1)$$

where μ is the mobility, C_i the insulator capacitance, and V_T is the threshold voltage. The mobility can be estimated from the transfer characteristic, Figure 8b, by deriving Equation 1 with respect to V_G.

$$\mu = \frac{L}{W C_i V_D}\frac{\partial I_D}{\partial V_G} \quad (2)$$

We note that Equation 2 is only valid if μ does not depend on V_G, which appears to be true in all cases except when V_G is below –3 V, where the mobility levels-off at around 0.0035 cm^2 V^{-1} s^{-1}. This number can be compared to mobility found in the literature for parent compounds. In the case of 4T, reported values range between 0.001[18] and 0.01 cm^2 V^{-1} s^{-1}.[19] Higher mobility, up to 0.025 cm^2 V^{-1} s^{-1}, has been obtained with dihexylquaterthiophene (DH4T), where the 4T molecule is substituted with a hexyl chain at both ends.[20] In all cases, molecules stand upright on the gate insulator, so the reported mobility corresponds to charge transport perpendicular to the

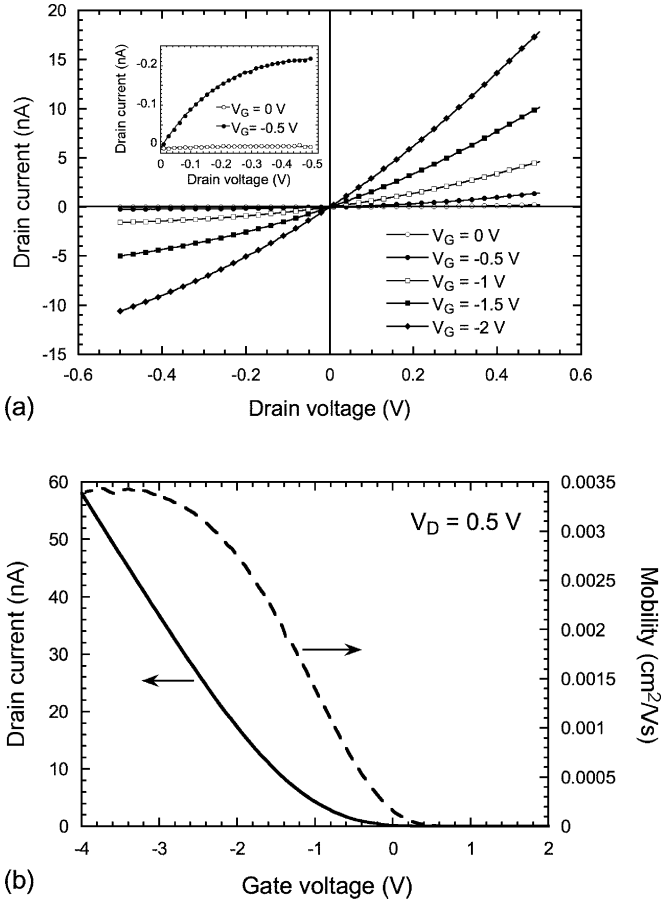

Figure 8. a) Output characteristics of a neat SAM-based transistor for gate voltages ranging between 0 and –2 V. The channel length is 60 nm, the channel width 10 μm, and the capacitance of the insulator 75 nF cm^{-2}. The drain-voltage scan was limited to ±0.5 V because of source–drain leaks occurring at higher voltages. The inset shows the characteristics at $V_G = 0$ and $V_G = -0.5$ V; the curves are restricted to a drain voltage between 0 and –0.5 V, and the axes have been reversed. b) Transfer characteristic of the same device at $V_D = 0.5$ V (left axis). The mobility (right axis) was extracted from the derivative of the I_D–V_G curve.

chains. The mobility in the SAM appears to be slightly lower than that reported for both the unsubstituted and dihexyl substituted oligomers. A tentative explanation is that the 4T-MEOA molecules are chemically attached to the substrate through the carboxylic acid group, thus inducing less dense packing than that found in vapor deposited films. We note that such a reduction of the mobility is a general rule in short channel OTFTs.[2,3]

For the top-contact transistors, 173 devices were measured in a controlled atmosphere (water and oxygen < 0.1 ppm). Most of the devices (153, or 88 %) did not show any signal. For 12 devices (7 %) the electrodes were short-circuited, i.e., the *I*–*V* curves were ohmic with a current of around 1 mA at 1 V (probably because of lithography problems). Only seven samples (4 %) displayed a current of ca. 100 nA and non-ohmic characteristics. Of these seven samples, two samples (1.1 %) clearly showed a field-induced modulation of the drain current as shown in Figure 9. From Equation 2, the maximum mobility for the 3T SAM transistor is estimated around 8×10^{-4} $cm^2 V^{-1} s^{-1}$ (at $V_G < -2$ V). At $V_D = -2$ V, the on–off ratio approaches 5,

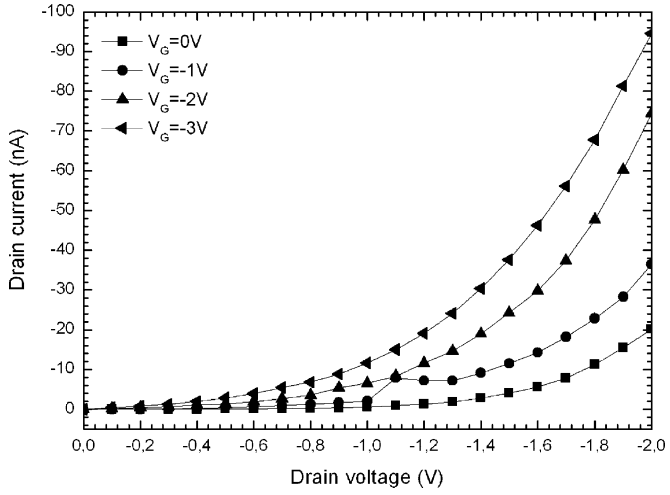

Figure 9. Output characteristics of a top-contact 3T SAM transistor. The channel length is 100 nm and the channel width is 20 µm.

and at $V_D = -0.5$ V it is ca. 65. As expected, the mobility is slightly lower than for the 4T SAM transistor (mobility increases with the length of the oligomer). It is worth pointing out that because to date, no mobility has been reported for vapor deposited 3T films, this number can be regarded as the first one for this oligothiophene.

2.4. Electrostatic Force Microscopy of the SAMs

Additional electrical characterization of 4T-MEOA SAMs was done by electrostatic force microscopy (EFM). Charge carriers were locally injected through the apex of the tip, and the resulting distribution and concentration of injected charges was measured by EFM following a protocol already used for pentacene monolayers and DNA molecules.[21,22] The EFM image and profile (Fig. 10) show that holes are more readily in-

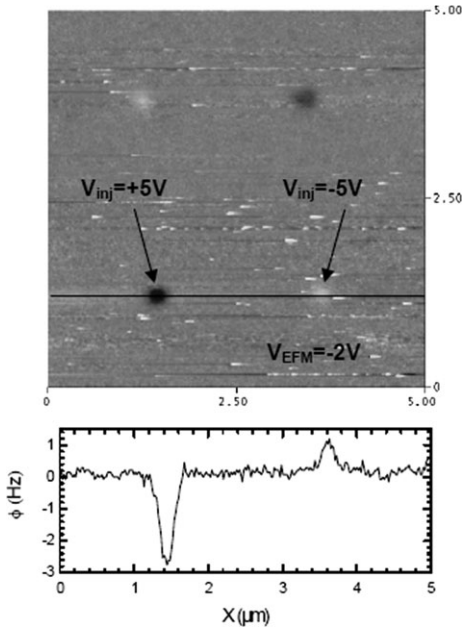

Figure 10. EFM image and profile of charges. Electrons are injected at V_{inj} –5 V and holes at +5 V from the tip gently contacted to the SAM with a typical 2 nN contact force for 2 min. Injection was done twice to check reproducibility. EFM measurements were done at a tip bias $V_{EFM} = -2$ V and a tip-to-surface distance $z = 40$ nm. EFM images are sensitive to the interaction between the charge Q stored in the sample and the capacitive charge at the tip apex. The EFM cantilever frequency shift is either positive or negative, and varies as $Q \times V_{EFM}$. $Q \times V_{EFM} > 0$ (repulsive interaction) corresponds to a positive frequency shift (bright features in the image). By contrast, $Q \times V_{EFM} < 0$ (attractive interaction) corresponds to a negative frequency shift and gives dark features in the image.

jected than electrons (hole-to-electron ratio ca. 2.8). Additionally, injection is isotropic, but holes spread over a larger range (ca. 0.58 µm) than electrons (ca. 0.41 µm). Note that these ranges exceed the spatial resolution of the EFM (ca. 50 nm in our case). A hole-to-electron asymmetry was also observed on a reference alumina sample (no SAM) but with a lower magnitude for both the charge density (hole-to-electron ratio ca. 2) and delocalization length (hole-to-electron ratio ca. 1). These results infer that holes can diffuse into the SAMs over distances of several hundreds of nanometers while electrons cannot, which is in agreement with the p-type field effect in devices with channel length lower than 100 nm. The delocalization length in the SAM is lower than that found in pentacene monolayer (a few micrometers),[22] which also agrees with the lower mobility in 4T-MEOA.

3. Conclusion

We have demonstrated the possibility of making a well-behaved organic transistor where the semiconductor is reduced to a single layer attached to the gate insulator. The failure to do so in some cases, can be attributed to either lack of charge transport in the monolayer, or deficient electrical contact between the semiconductor layer and the source and drain elec-

ADVANCED FUNCTIONAL MATERIALS

trodes. Improvement in charge transport was obtained by reducing the channel length down to a size where the number of defects along the path from source to drain was limited to less then or equal to three. Although a dependable technique to achieve good contacts is still to be found, this result is important because it provides evidence that the poor performance obtained in most cases does not come from inherently poor charge transport or difficulty to inject charges in the single layer. This work also shows that making an organic transistor with a semiconductor film reduced to a single layer is an alternative means to obtain devices that operate at very low voltages.

4. Experimental

4.1. Synthesis of 4T-MEOA

*5-Formyl-2,2′-bithiophene (**1**)*: Phosphorous oxychloride (9.5 mL, 101.8 mmol) was added to a solution of bithiophene (15.1 g, 90.6 mmol) and dimethylformamide (DMF; 8 mL, 101.8 mmol) in 150 mL of 1,2-dichloroethane at 0 °C. The solution was gradually warmed to room temperature and refluxed overnight. After cooling to room temperature, the solution was hydrolyzed with 300 mL of brine solution. It was extracted three times with 100 mL of dichloromethane. The organic phase was washed with water, dried and concentrated under reduced pressure. The residue was separated by chromatography on silica gel using ethyl acetate/hexane (50:50) to yield a light brown solid (16.8 g 93 %). ^{1}H NMR (200 MHz, $CDCl_3$, ppm): δ 9.86 (s, 1H), 7.66 (d, J = 4 Hz, 1H), 7.36 (d, J = 4 Hz, 2H), 7.25 (d, J = 4 Hz, 1H), 7.07 (t, J = 4 Hz, 1H). ^{13}C NMR (50 MHz, $CDCl_3$, ppm): δ 146.5, 141.7, 135.5 (3C-quarternary (q)), 137.3, 128.3, 127.1, 126.7 (5CH-aromatic (aryl)). MS: m/z = 194 (100), 193 (89), 171 (17), 121 (61).

5-(Trimethylstannyl)-2,2′-bithiophene: In a dried three-necked flask, 8.31 g of 2,2′-bithiophene (50 mmol) was dissolved in 30 mL of distilled THF. The solution was cooled to –78 °C and 20 mL of a solution of BuLi (2.5 M in hexane; 50 mmol) was added dropwise under argon. The mixture was stirred for 30 min and a solution of $(CH_3)_3SnCl$ (10 g, 50.2 mmol, 1.1 eq.) in 30 mL of distilled tetrahydrofuran (THF) was added dropwise under argon. Then the solution is allowed to warm up to room temperature and stirred for 12 h. After hydrolysis with 3 mL of water, the solvent was removed under reduced pressure. The resulting oil was diluted with diethylether (100 mL) and washed with a saturated solution of NaCl (100 mL). The layers are separated, the aqueous layer was washed twice with diethylether (2 × 50 mL) and the combined organic layers were washed again with a saturated solution of NaCl (2 × 50 mL). The organic phase was dried over $MgSO_4$, and the solvent removed under reduced pressure. A distillation under reduced pressure afforded a transparent oil (11.6 g, 70 %). ^{1}H NMR (200 MHz, $CDCl_3$, ppm): δ 7.23 (d, J = 3.5 Hz, 1H), 7.14 (d, J = 3.5 Hz, 2H), 7.03 (d, J = 3.5 Hz, 1H), 6.94 (t, J = 3.5 Hz, 1H), 0.33 (s, 9H).

*2-Bromo-5-formyl-2,2′-bithiophene (**2**)*: To a solution of **1** (7 g, 36 mmol) in 125 mL of chloroform was added sodium bicarbonate (3.36 g, 40 mmol), followed by addition of a solution of bromine in chloroform (82.6 mL, 0.51 M, 40 mmol) over 1 h. The reaction mixture was stirred for 12 h at room temperature and filtrated. The filtrate was washed with water, dried, and concentrated. The crude product (9.48 g, 96 %) was used in the next step without purification. ^{1}H NMR (200 MHz, $CDCl_3$, ppm): δ 9.86 (s, 1H), 7.66 (d, J = 4 Hz, 1H), 7.18 (d, J = 4 Hz, 1H), 7.10 (d, J = 4 Hz, 1H), 7.04 (t, J = 4 Hz, 1H). MS: m/z 274 (100), 271 (55), 245 (11), 201 (26), 164 (18).

*2-Bromo-5-methylalcohol-2,2′-bithiophene (**3**)*: To a solution of **2** (8.48 g, 30.9 mmol) in 235 mL of THF was added 6 g of $NaBH_4$ (159 mmol). The reaction mixture was stirred for 2 h at room temperature, and the solvent removed under reduced pressure. 200 mL of water was added and the solution was acidified to pH 2 with 6 M HCl at 0 °C. The obtained suspension was filtrated and dried (7.82 g, 92 %). The product was used in the next step without further purification. ^{1}H NMR (200 MHz, deuterated dimethylsulfoxide (d_6-DMSO), ppm): δ 7.19 (d, J = 3.5 Hz, 1H), 7.13 (d, J = 3.5 Hz, 1H), 7.08 (d, J = 3.5 Hz, 1H), 6.90 (d, J = 3.5 Hz, 1H), 5.56 (t, J = 5.7 Hz, 1OH), 4.60 (d, J = 5.7 Hz, 2H). ^{13}C NMR (50 MHz, $CDCl_3$, ppm): δ142.5, 137.9, 136.0, 110.5 (4C-q), 130.6, 126.1, 123.8, 123.6 (4CH-ar), 60.1 ($1CH_2$); MS m/z = 276 (100), 257 (100) 243 (38), 177 (18), 166 (45).

*2-Bromo-2,2′-bithiophene-5-methyletheroctanoic Acid (**4**)*: To a cold solution of NaH (1 g, 24.81 mmol) in 30 mL of DMF, was added dropwise a DMF solution of 8-bromooctanoic acid (2 g, 9 mmol). The reaction was stirred at 0 °C for 30 min, and a DMF solution (30 mL) of **3** (3 g, 10.8 mmol) was added dropwise. The reaction mixture was stirred at room temperature for 48 h, and the solvent removed under reduced pressure. The crude product was dissolved in diethyl ether and washed twice with water. The aqueous layer was extracted twice with diethyl ether. The combined aqueous phases were acidified to pH 1 with 6 M HCl at 0 °C and the aqueous phase extracted twice with ethyl acetate. The combined organic phases were dried over $MgSO_4$ and the solvent was removed under reduced pressure. Purification on silica gel with a gradient of ethyl acetate/petroleum ether (4:1 to 4:2) afforded a yellow–green powder (1.82 g, 61 %). ^{1}H NMR (200 MHz, $CDCl_3$, ppm): δ 6.95 (d, J = 3.6 Hz, 2H), 6.87 (2d, J = 3.5 Hz, 2H), 4.61 (s, 2H), 3.48 (t, J = 6.4 Hz, 2H), 2.34 (t, J = 7.4 Hz, 2H), 1.60 (m, 4H), 1.34 (m, 6H). ^{13}C NMR (50 MHz, $CDCl_3$, ppm): δ 179.7, 141.2, 139.0, 135.5, 11.0 (5Cq), 130.5, 126.7, 123.6, 123.4 (4CHar), 70.2, 67.3, 39.9, 29.5, 29.0, 25.9, 24.5 ($8CH_2$); MS m/z 418 (40), 337 (10), 273 (28), 259 (100), 195 (17).

*8-Methylether-α,α′-quaterthiopheneoctanoic Acid (**5**)*: A solution of 5-(trimethylstannyl-2,2′-bithiophene (1.7 g, 5.2 mmol) and **4** (2 g, 4.8 mmol) in 47 mL of DMF was deaerated with argon for 20 min, then 70 mg of bis(triphenylphosphine)palladium(II) dichloride was added. The mixture was stirred for 12 h at 90 °C. The DMF was removed under reduced pressure and the resulting brown powder ultrasonically washed in sequence with cyclohexane, diethyl ether, and ethyl acetate to afford a brown powder (1.21 g, 50 %). Gas chromatography–mass spectroscopy showed that the crude product was contaminated with 5 % of α,α′-quaterthiophene formed via Stille homocoupling. Analytically pure 8-methylether-α,α′-quaterthiopheneoctanoic acid was obtained by repeating the purification process. ^{1}H NMR (200 MHz, d_6-DMSO, ppm): δ 7.54 (d, J = 5.2 Hz, 1H), 7.36 (d, J = 2.4 Hz, 1H), 7.29 (m, 4H), 7.21 (d, J = 3.3 Hz, 1H), 7.11 (t, J = 5.2 Hz, 1H), 7.01 (d, J = 3.3 Hz, 1H), 4.60 (s, 2 H), 3.44 (t, J = 6.4 Hz, 2H), 2.18 (t, J = 7.4 Hz, 2H), 1.48 (m, 4H), 1.26 (m, 6H). MS m/z: 358 (24), 344 (71), 343 (100).

4.2. Preparation of SAMs

Solutions of 4T-MEOA were prepared in distilled benzene that was purified with alumina balls activated prior to use at 400 °C for 3 h. The preparation of the alumina substrates included cleaning in a homemade UV/ozone cleaner for 30 min, followed by etching in pure sulfuric acid (Merck, 98 %) for 30 s and thorough rinsing in ultrapure water (Elga UHQ II).

Two methods were used to deposit the SAM. The first one consisted of dipping the substrate in the solution immediately after the cleaning process. Under these circumstances, the thickness of the layer was controlled through the dipping time (typically 10–15 min for one monolayer). In the second method, or "calibrated-drop-casting", a droplet that contains the exact amount of molecules needed to deposit the desired number of layers was dropped on the substrate. The substrate is then placed in a tube under saturated pressure of the solvent. The evaporation time (typically 1 h) of the solvent is controlled by the size of the aperture of the tube. Note that the time taken using this method is longer than that taken in the dipping method. The last step consisted of thermal baking (48 h at 50 °C) under argon.

The SAMs were characterized by PMIRRAS. The set up comprised a Nicolet 860 FTIR (Thermo Electron) spectrometer equipped with the commercially available photoelastic modulation (PEM) module including a ZnSe photoelastic modulator.

ADVANCED FUNCTIONAL MATERIALS

Characterization of the Transistors: The electrical characterization of the bottom-contact 4T-MEOA transistors was performed under ambient conditions on a Suss-Microtec PM5 manual probe station connected to a Keithley 4200-SCS semiconductor characterization system. For the top-contact devices, the probe station was installed inside a MBRAUN glovebox and connected to an Agilent 4156 semiconductor parameter analyzer.

Received: February 23, 2006
Revised: April 27, 2006
Published online: January 26, 2007

[1] J. Collet, O. Tharaud, A. Chapoton, D. Vuillaume, *Appl. Phys. Lett.* **2000**, *76*, 1941.
[2] Y. Zhang, J. R. Petta, S. Ambily, Y. Shen, D. C. Ralph, G. G. Malliaras, *Adv. Mater.* **2003**, *15*, 1632.
[3] L. Wang, D. Fine, T. Jung, D. Basu, H. von Seggern, A. Dodabalapur, *Appl. Phys. Lett.* **2004**, *85*, 1772.
[4] J. Paloheimo, P. Kuivalainen, H. Stubb, E. Vuorimaa, P. Yli-Lahti, *Appl. Phys. Lett.* **1990**, *56*, 1157.
[5] L. Aguilhon, J. P. Bourgoin, A. Barraud, P. Hesto, *Synth. Met.* **1995**, *71*, 1971.
[6] G. F. Xu, Z. A. Bao, J. T. Groves, *Langmuir* **2000**, *16*, 1834.
[7] C. R. Kagan, A. Afzali, R. Martel, L. M. Gignac, P. M. Solomon, A. G. Schrott, B. Ek, *Nano Lett.* **2003**, *3*, 119.
[8] G. S. Tulevski, Q. Miao, M. Fukuto, R. Abram, B. Ocko, R. Pindak, M. L. Steigerwald, C. R. Kagan, C. Nuckolls, *J. Am. Chem. Soc.* **2004**, *126*, 15 048.
[9] A. Ulman, *An Introduction to Ultrathin Organic Films: From Langmuir–Blodgett to Self-Assembly*, Academic, San Diego, CA **1991**.
[10] Y. Y. Lin, D. J. Gundlach, T. N. Jackson, S. F. Nelson, *IEEE Trans. Electron Devices* **1997**, *44*, 1325.
[11] A. Facchetti, M. Mushrush, H. E. Katz, T. J. Marks, *Adv. Mater.* **2003**, *15*, 33.
[12] S. H. Kim, J. H. Lee, S. C. Lim, Y. S. Yang, T. Zyung, *Jpn. J. Appl. Phys., Part 2* **2004**, *43*, 60.
[13] M. Halik, H. Klauk, U. Zschieschang, G. Schmid, C. Dehm, M. Schuetz, S. Maisch, F. Effenberger, M. Brunnbauer, F. Stellacci, *Nature* **2004**, *431*, 963.
[14] D. L. Allara, R. G. Nuzzo, *Langmuir* **1985**, *1*, 45.
[15] P. Lang, R. Hajlaoui, F. Garnier, B. Desbat, T. Buffeteau, G. Horowitz, A. Yassar, *J. Phys. Chem.* **1995**, *99*, 5492.
[16] S. Lenfant, D. Guerin, F. Tran Van, C. Chevrot, S. Palacin, J. P. Bourgoin, O. Bouloussa, F. Rondelez, D. Vuillaume, *J. Phys. Chem. B* **2006**, *110*, 13 947.
[17] G. J. Kluth, M. M. Sung, R. Maboudian, *Langmuir* **1997**, *13*, 3775.
[18] W. A. Schoonveld, R. W. Stok, J. W. Weijtmans, J. Vrijmoeth, J. Wildeman, T. M. Klapwijk, *Synth. Met.* **1997**, *84*, 583.
[19] R. Hajlaoui, G. Horowitz, F. Garnier, A. Arce-Brouchet, L. Laigre, A. El Kassmi, F. Demanze, F. Kouki, *Adv. Mater.* **1997**, *9*, 389.
[20] T. Muck, V. Wagner, U. Bass, M. Leufgen, J. Geurts, L. W. Molenkamp, *Synth. Met.* **2004**, *146*, 317.
[21] T. Heim, T. Melin, D. Deresmes, D. Vuillaume, *Appl. Phys. Lett.* **2004**, *85*, 2637.
[22] T. Heim, K. Lmimouni, D. Vuillaume, *Nano Lett.* **2004**, *4*, 2145.